Journal of Power Sources 190 (2009) 103–109

Contents lists available at ScienceDirect

Journal of Power Sources

journal homepage: www.elsevier.com/locate/jpowsour

Sensing electrodes for failure diagnostics in fuel cells

O. Herrera[a,b], W. Mérida[a,b,*], D.P. Wilkinson[a,c,**]

[a] Clean Energy Research Centre, University of British Columbia, Vancouver, BC, Canada V6T 1Z4
[b] Department of Mechanical Engineering, University of British Columbia, Vancouver, BC, Canada V6T 1Z4
[c] Department of Chemical and Biological Engineering, University of British Columbia, Vancouver, BC, Canada V6T 1Z3

ARTICLE INFO

Article history:
Received 12 June 2008
Received in revised form 7 August 2008
Accepted 8 August 2008
Available online 22 August 2008

Keywords:
PEM fuel cell
Failure modes
Diagnostics
Sensing electrodes

ABSTRACT

The durability and reliability of fuel cell products need to be improved. The lack of early diagnosis and failure-prevention techniques is one of the limiting factors. We present a non-invasive method for the early diagnosis of flooding, dehydration and low fuel stoichiometry (three common failure modes). Our method is based on microsensing electrodes (SE) that are placed at appropriate locations in a single cell. These electrodes have a characteristic potential response to each of the failure modes, which enables detection prior to overall fuel cell failure. The specific features in the measured responses (or combinations thereof) can be used to discern between different failure modes, and initiate corrective actions.

1. Introduction

Fuel cell products are at the demonstration/early commercialization stage. In order to improve their performance and reliability, early diagnosis and failure prevention are necessary. Some of the most common failure modes in proton exchange membrane fuel cells (PEMFCs) are fuel cell flooding, membrane dehydration, catalyst poisoning, and low reactant supply, often leading to reactant starvation. The failures reduce the performance of the fuel cell and can cause permanent damage. Flooding reduces the mass transport of reactants to the reaction sites; dehydration increases the ohmic resistances of the membrane and can lead to irreversible damage; catalyst poisoning reduces the active catalyst sites with contaminants such as CO or other organic compounds; and starvation can lead to fuel cell reversal and carbon corrosion.

It is important to develop a fundamental understanding of fuel cell failure modes. Several techniques have been used to investigate PEMFC failures. These include magnetic resonance imaging [1-5], X-ray [6,7], neutron imaging [8,9] and visualisation in transparent fuel cells [10,11]. One of the limitations of these techniques is the need for cell modification(s) or specialised equipment and facilities. These limitations prevent them from being used for *in situ* diagnostics.

Less invasive methods for fuel cell failure mode diagnosis include impedance spectroscopy [12–18], pressure drop monitoring (e.g., caused by flooding) [19–22], and ohmic resistance measurement [23]. For CO poisoning, the diagnostic tools include: ceramic sensors [24–26] and sensors based on modified membranes and catalysts [27–31]. These and other diagnostic tools and methods can be used in real fuel cell applications, but the implementation costs are still high and they can only be used for one type of failure mode. Wilkinson et al. have discussed an interesting *in situ* diagnostic tool based on sensor cells [32].

Our approach is to use sensing electrodes (SE) as a diagnostic tool; in this case, platinum wires that provide a specific, location-specific response to different failure modes. We base this approach on the effect of local conditions on PEMFC performance. For example, gradients between the cell inlet and outlet in the membrane's water content, temperature, pressure, and reactant concentrations play a major role in the uneven distribution of current across the cell's active area. The impact of gradients on cell performance has been shown by Wilkinson and St-Pierre [33] and in other papers by distributed measurements [34–41]. The potential response of the SEs also depends on these conditions, and if placed in the appropriate locations (e.g., the fuel inlets and outlets), they can be used as diagnostic tools.

In this paper, we present the response of two sensing electrodes (SEs) one at the fuel inlet (SE_{in}) and the other at the outlet (SE_{out})

* Corresponding author at: Clean Energy Research Centre, University of British Columbia, Vancouver, BC, Canada V6T 1Z4. Fax: +1 604 822 2403.
** Co-corresponding author.
E-mail addresses: omarhh@interchange.ubc.ca (O. Herrera), walter.merida@ubc.ca (W. Mérida), dwilkinson@chml.ubc.ca (D.P. Wilkinson).

0378-7753/$ – see front matter © 2008 Elsevier B.V. All rights reserved.
doi:10.1016/j.jpowsour.2008.08.034

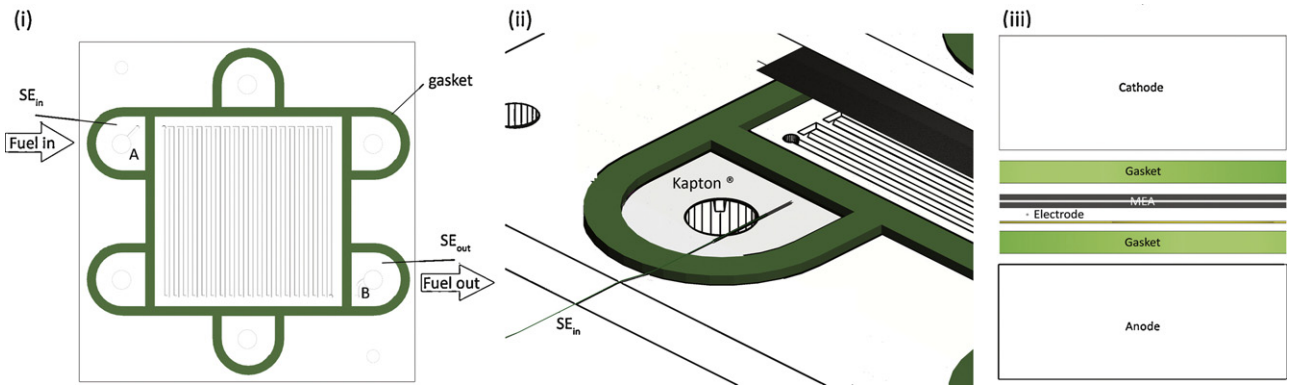

Fig. 1. (i) Placement of the SE_{in} and the SE_{out}, in chambers A and B, respectively, in contact with the solid electrolyte. (ii) Placing of SE_{in} protected by Kapton®. (iii) Exploded side view of an electrode chamber. The chambers are connected through ports to the active fuel cell flow field.

that have characteristic potential responses to undesirable conditions in the fuel cell (flooding, dehydration and fuel starvation). The characteristic potential response of the sensing electrodes occurs before the overall cell voltage is affected and it enables the early diagnosis of these failure modes.

2. Experimental

2.1. Sensing electrode and fuel cell testing

The sensing electrodes consisted of a 50-μm platinum wire with a 25-μm Teflon® coating. The Teflon® was removed at the wire tip to expose 2 mm of platinum that was cleaned and then platinized according to the procedure described by Ives and Janz [42]. In this paper two sensing electrodes were used, as shown in Fig. 1: one sensing electrode in the inlet of the fuel stream (SE_{in}) inside fuel chamber A and one sensing electrode in the outlet of the fuel stream (SE_{out}) in fuel chamber B. The sensing electrodes were in contact with hydrogen that entered and exited the cell through their respective ports. These electrodes are sensitive to the local environmental conditions, such as, humidity, temperature, concentration, etc. The sensing electrodes were fixed in the chambers by placing them between a layer of Kapton® and the membrane, and then compressing the assembly to 120 psi (see Fig. 1). These Kapton® layers prevented short-circuiting of the electrodes with the graphite plates. Our experimental results indicated that there was no change in the electrode potentials with positioning within the chambers.

The SEs were connected to the anode and to the cathode and the voltage differences between SE_{in} and SE_{out} were obtained as shown in Fig. 2. With this arrangement we were able to see how different conditions affected the anode and the cathode and also use the SE_{in} and SE_{out} as diagnostic tools for different hydration conditions and fuel stoichiometric ratios for a PEMFC. The potentials were measured and recorded using a Solartron Analytical 1470E CellTest System potentiostat/galvanostat. Each sensing electrode was connected to the anode and the cathode to allow anode and cathode potentials, and the fuel cell potentials to be recorded.

The fuel cell shown in Fig. 3 had thermocouple ports that were used to map the local temperature. It also had a pneumatic piston for compression that distributed the pressure evenly across the cell. All the experiments were done with a custom made 49 cm^2 E-Tek MEA with 0.3 mg cm^{-2} loading of Pt/C on the anode and 0.7 mg cm^{-2} Pt/C on the cathode with a Nafion® 115 membrane. We chose this type of MEA without a microporous layer because it is more sensitive to water management issues and the failures are easier to simulate. The fuel cell experiments were carried out with a 1 kW Arbin Instruments Fuel Cell Test Station (FCTS) with hydrogen and air as the fuel, respectively. The test station controlled the flow rate, humidity, temperature and pressure of the gases supplied. To induce the failures, the fuel flow rate was gradually decreased to create fuel starvation and the dew point temperatures of the fuel and oxidant inlet lines were modified to promote flooding or dehydration.

3. Results and discussion

To test the stability of the electrodes, the fuel cell was run at different current densities and at open circuit voltage for more than 10 h (2 h at each setting), as shown in Fig. 4. The response of the sensing electrodes at normal conditions (sum-

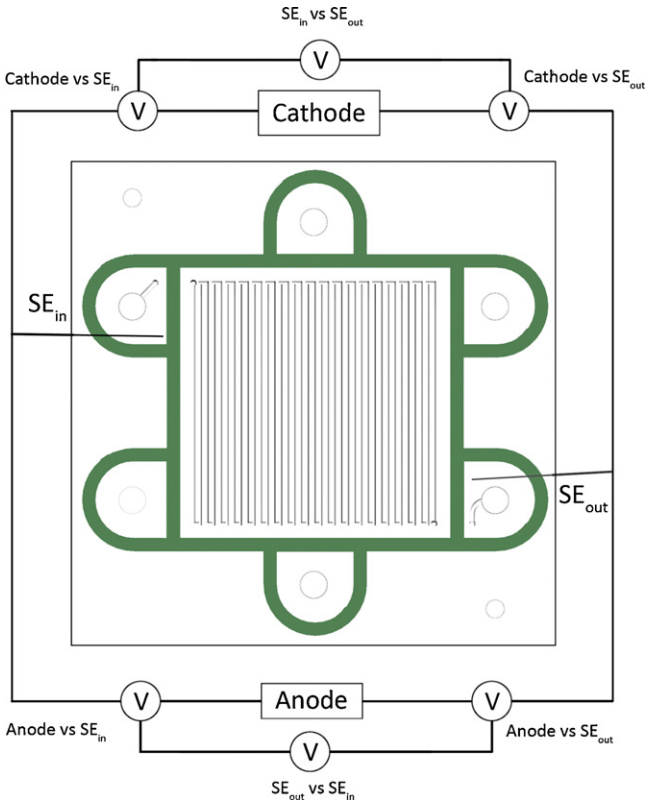

Fig. 2. Connection diagram for the SE_{in} and SE_{out}. The voltages were measured versus the anode and the cathode, and the difference between the two electrodes was calculated.

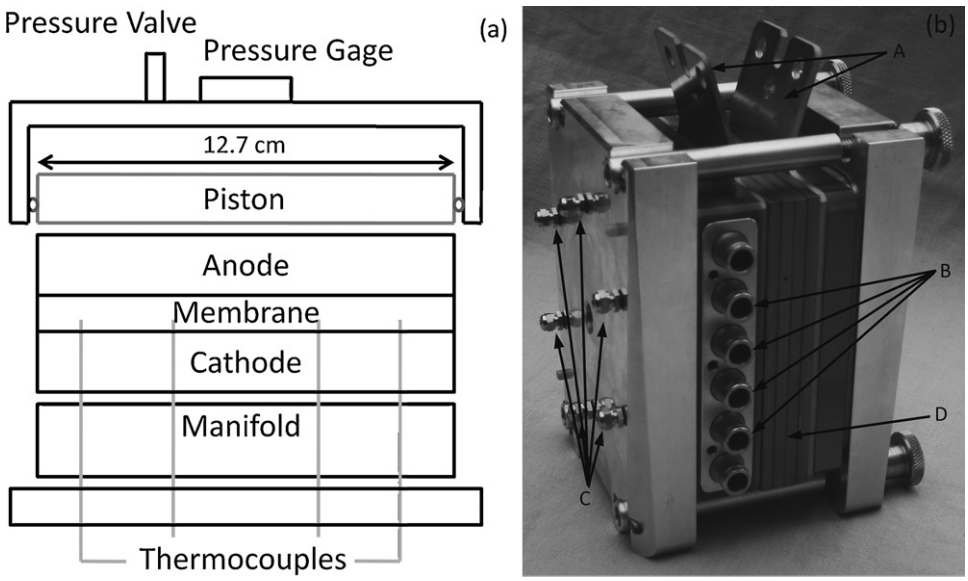

Fig. 3. (a) Diagram of research fuel cell components. (b) Picture of research fuel cell, with components identified: (A) current collectors, (B) gas ports, (C) thermocouple ports, and (D) bipolar plates.

Table 1
Conditions of fuel cell testing

Arbin test station	1 kW	
	Anode	Cathode
Gas	Hydrogen	Air
Outlet back pressure (atm)	3	3
Gas temperature (K)	348	348
Stoichiometry	2	3
Dew point temperature (K)	348	348
Cell temperature (K)	348	

The variables were controlled with an Arbin test station (1 kW) and modified to create failure conditions for the fuel cell.

marized in Table 1) depended only on the operating point of the fuel cell without adding any noise, demonstrating their reliability and stability. The potential difference between the SE_{in} and the SE_{out} was also constant at normal conditions, as shown in Fig. 5. In this figure, the general treatment of the data is also shown. Each point on a voltage plateau is an average of at least 15 min at a given condition. The standard deviation for each point was also calculated and shown in Fig. 5. These average potential responses and standard deviations are different during different operating conditions. During normal conditions, the standard deviations from the SEs and from the fuel cell are very similar. When a failure is induced, the standard deviations of the Cathode vs. the SEs are larger than the fuel cell's and depending on the failure, the standard deviation is smaller or larger. The potential response and standard deviations of the Cathode vs. the SEs at different conditions (normal, dehydration and flooding) are portrayed in Fig. 6. For dehydration, the relative humidity (RH) was set at 10% for both gases. For flooding, the gas temperature (GST) was set at 75 °C and the dew point temperature (DPT) was set to 90 °C. In both cases the system ran for 1 h at 500 mA cm^{-2} at the given conditions of flooding and dehydration before recording the polarization curve points. The different conditions affect the anode and the cathode, as well as, the sensing

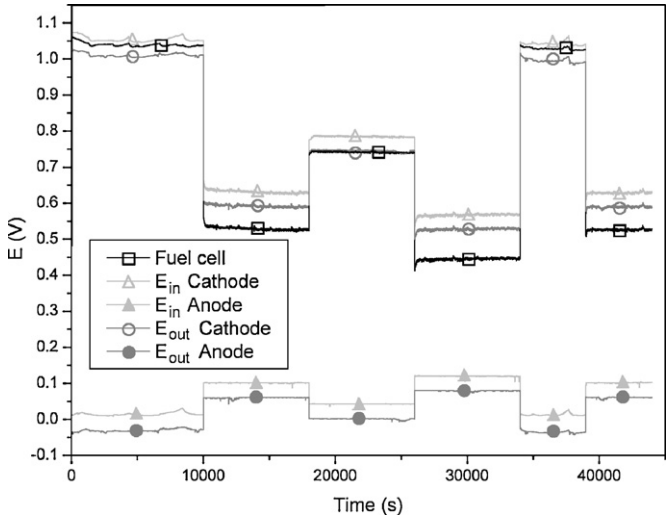

Fig. 4. Stability of sensing electrodes in a fully humidified fuel cell (Table 1 conditions) at different current densities for more than 10 h.

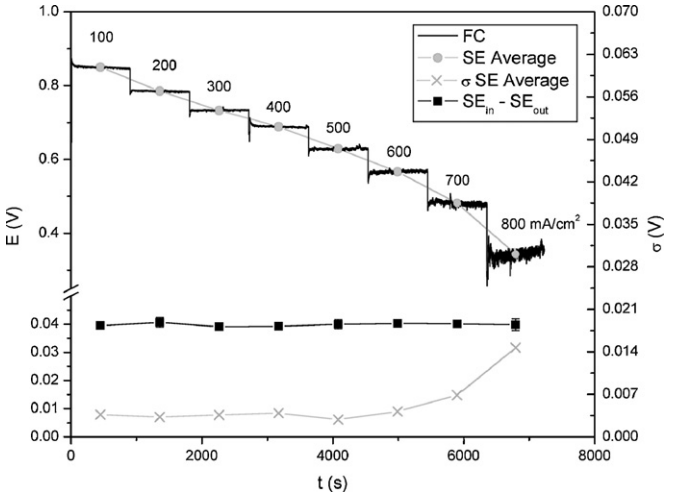

Fig. 5. General treatment of the data obtained with SEs. The average and standard deviation of at least 15 min per point was calculated. Also, the potential difference between SE_{in} and SE_{out} is shown.

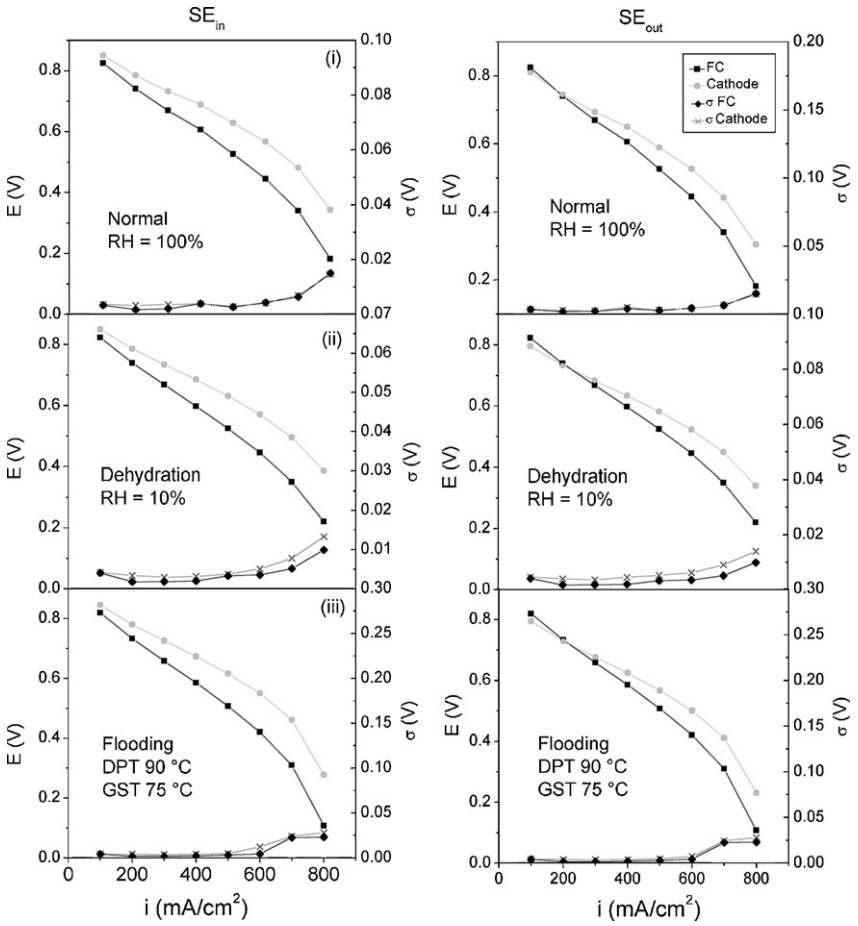

Fig. 6. Potential responses and standard deviation of SE_{in} and SE_{out} at different conditions: normal (i), dehydration (ii), and flooding (iii).

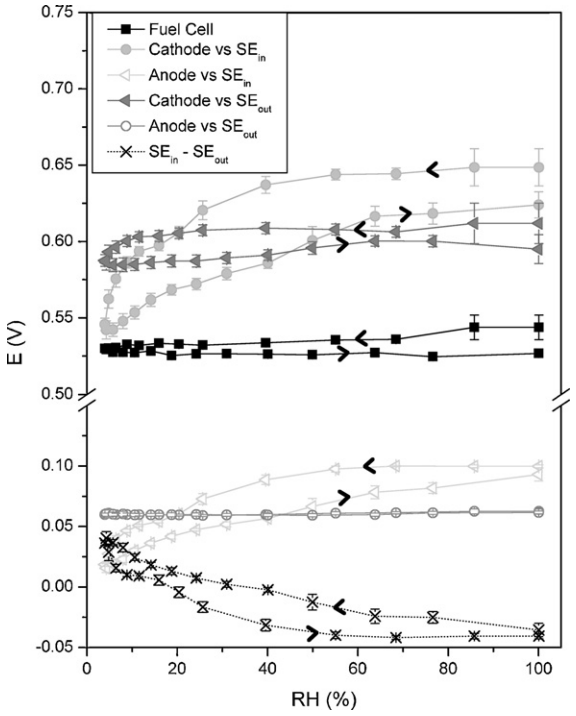

Fig. 7. Potential response of SE_{in} and SE_{out} at different RH. The RH is gradually reduced to a minimum of 5% and then back to 100%.

electrodes. The SE_{in} is more sensitive to the effects of drying, while the SE_{out} is more sensitive to the effects of flooding and low fuel stoichiometry.

Fig. 7 shows the effect of relative humidity on the SE_{in} and the SE_{out}. The SE_{in} local conditions change the most, affecting the potential response of the electrode before the conditions affect the fuel cell's overall potential or the potential of the SE_{out}. The anode vs. SE_{out} potential response has less than a 10-mV difference between points. The local conditions for that electrode do not vary during the experiment because the fuel cell produces enough water to keep the exit conditions almost constant. The anode and cathode vs. SE_{in} change significantly with relative humidity. The anode vs. the SE_{in} changes less than the cathode vs. the SE_{in}, likely because as the membrane/ionomer dries, the proton concentration is reduced limiting the oxygen reduction reaction. The drying effects appear to be irreversible and lead to hysteresis. After a 15-h experiment where the dew point temperature was reduced 5 °C every 30 min down to a minimum of 5%RH and then increased at the same rate to the original level, the final fuel cell potential decreased by more than 20 mV over the experimental current density range.

The information that can be obtained from the anode and cathode versus the sensing electrodes is very valuable. Nevertheless, in order to diagnose and ultimately prevent the failure only the potential difference between the sensing electrodes, SE_{in} and the SE_{out} is needed, as shown in Fig. 7. In Fig. 8, the potential response to flooding of the SE_{in}–SE_{out} is shown. The dew point temperature and the pressure difference between the inlet and outlet of the anode and the cathode are also displayed. Flooding can also

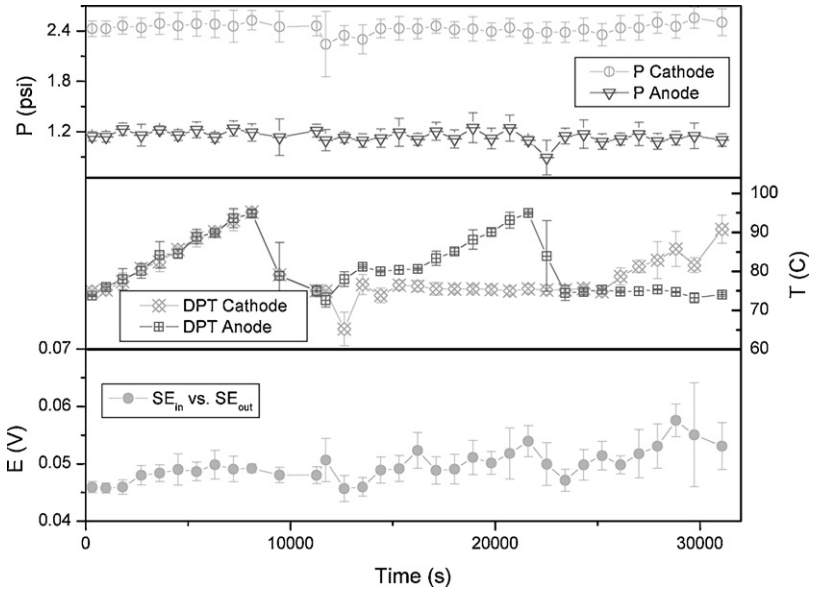

Fig. 8. Potential response SE_{in} vs. SE_{out} during flooding conditions. The pressure differences between the inlet and the outlet of both the anode and the cathode confirm the potential response results.

be diagnosed by the pressure difference between the anode inlet and the anode outlet. The SE_{in}–SE_{out} also shows that the potential oscillates with higher response when only the cathode is flooded, but the pressure fluctuation is not as significant as in the other case. In general, pressure difference monitoring is not as sensitive a diagnostic tool as the precise voltage monitoring from the SEs.

For low fuel stoichiometry, the faster potential response is even more evident as shown in Fig. 9. The faster response of the SEs is due to their need for hydrogen to operate. The SE_{in} changes the most as the local conditions in that chamber are the first to be affected. It takes a change of stoichiometry of 0.03, in this case, more than one and a half hours, for the fuel cell to show a noticeable change on potential. The standard deviation is also constant until the potential change occurs. This failure is one of the most damaging ones, as the potential drops to zero as soon as there is a lack of hydrogen. If the lack of hydrogen persists, it can lead to fuel cell reversal (production of hydrogen with power consumption instead of consumption hydrogen and power generation). If the failure continues, the catalyst can be corroded and even the graphite plates can be damaged.

The SEs can prevent permanent damage to the fuel cell by diagnosing the failure before it affects the fuel cell, and providing sufficient time for corrective measures. If the potential of the

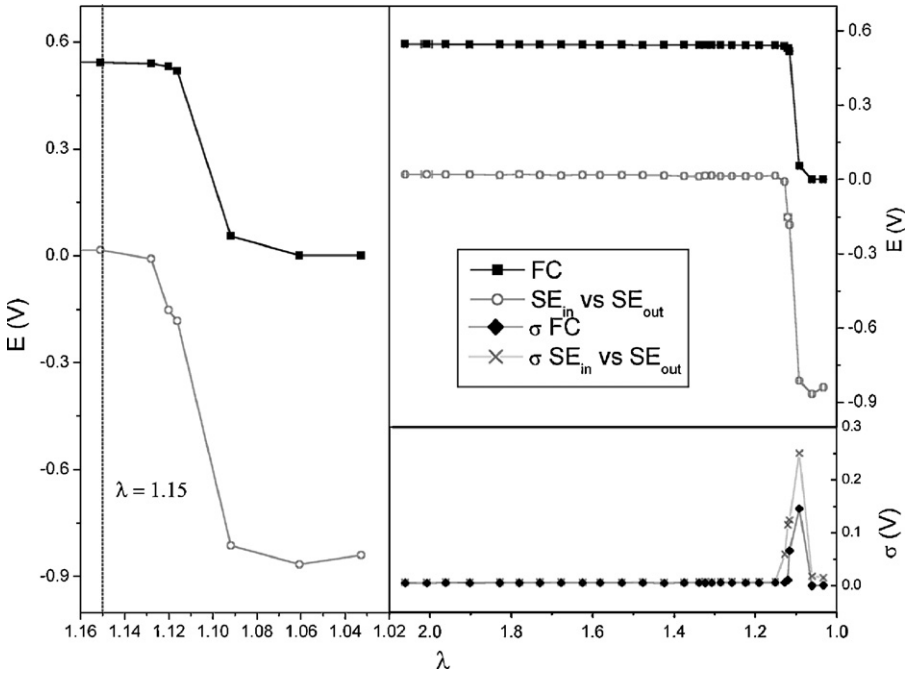

Fig. 9. Potential response of SE_{in} vs. E_{out} to gradual reduction of fuel stoichiometry. This potential difference shows an earlier response than the fuel cell.

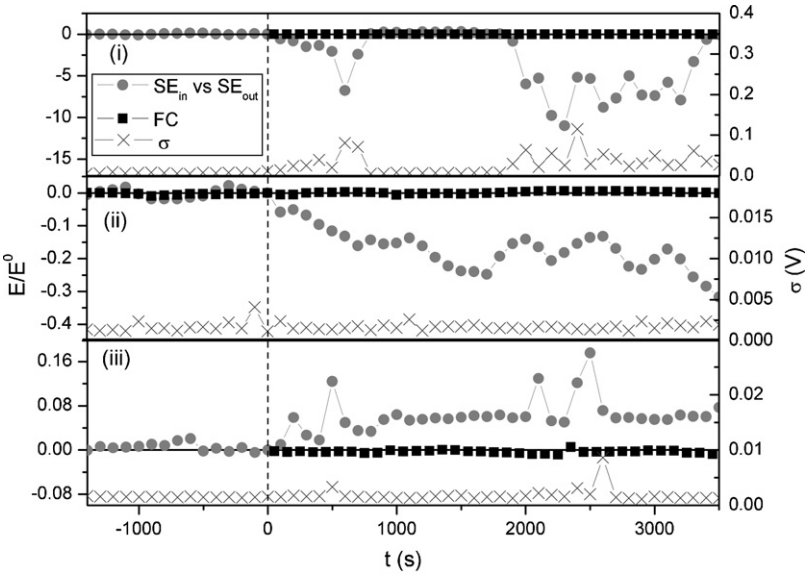

Fig. 10. Characteristic response under simulated low fuel stoichiometry (i), drying (ii) and flooding (iii). Time 0 is when the undesired conditions are detected by the SEs ($\lambda < 1.15$, RH < 60%, and dew point temperature 5° higher than the cell temperature). The fuel cell potential shows little variation while the potential difference between SE_{in} and SE_{out} is changing.

SE_{in} vs. SE_{out} (E) is divided by the electrode potential difference at normal conditions (E^0, $t = 0$), the SEs diagnosis can be done in 5 min for this experimental setup. It only requires averages of 100 s of data points where the standard deviation is also calculated to corroborate the diagnosis. Fig. 10 illustrates the effects of low fuel stoichiometry, dehydration, and flooding. If the potential difference between the SE_{in} and the SE_{out} is considerably negative with a high σ, then there is low fuel stoichiometry. If the potential difference between the SE_{in} and the SE_{out} is negative and the σ is practically constant, then there is drying. For flooding, the potential difference has to be positive and show peaks and the standard deviation (σ) must also present positive peaks. This information can be easily incorporated into the logic of a real time diagnosis system.

4. Conclusions

In this paper three failure modes were examined: flooding, dehydration and low fuel stoichiometry. Each failure mode had a characteristic response based on sensing electrode measurements prior to any changes in the overall cell voltage. Sensing electrodes can be used for early detection of many different types of failure modes. The SEs are sensitive to the local cell conditions, so their positioning in the cell is important. If the local conditions for the SEs change with respect to the operating conditions and associated failure mode, the SEs will have a potential response characteristic to that failure.

These type of electrodes can also be used as a quasi-reference to determine the anodic and cathodic contributions in a fuel cell, as well. The true potential of the sensing electrodes can only be known if the resistances are taken into account and the conditions for the electrode are known and constant.

Acknowledgments

This research was supported by the Natural Sciences and Engineering Research Council (NSERC) and the National Council of Science and Technology (CONACYT) of Mexico. The authors also like to acknowledge Tandem Technologies Inc. for the help in building the fuel cell.

References

[1] K.W. Feindel, S.H. Bergens, R.E. Wasylishen, J. Am. Chem. Soc. 128 (2006) 14192–14199.
[2] K.W. Feindel, L.P.A. LaRocque, D. Starke, S.H. Bergens, R.E. Wasylishen, J. Am. Chem. Soc. 126 (2004) 11436–11437.
[3] K. Teranishi, S. Tsushima, S. Hirai, Electrochem. Solid-State Lett. 8 (2005) A281–A284.
[4] S. Tsushima, K. Teranishi, S. Hirai, Electrochem. Solid-State Lett. 7 (2004) A269–A272.
[5] K.R. Minard, V.V. Viswanathan, P.D. Majors, L.-Q. Wang, P.C. Rieke, J. Power Sources 161 (2006) 856–863.
[6] V.R. Albertini, B. Paci, A. Generosi, S. Panero, M.A. Navarra, M. di Michiel, Electrochem. Solid-State Lett. 7 (2004) A519–A521.
[7] P.K. Sinha, P. Halleck, C.-Y. Wang, Electrochem. Solid-State Lett. 9 (2006) A344–A348.
[8] I.A. Schneider, D. Kramer, A. Wokaun, G.G. Scherer, Electrochem. Commun. 7 (2005) 1393–1397.
[9] A. Turhan, K. Heller, J.S. Brenizer, M.M. Mench, J. Power Sources 160 (2006) 1195–1203.
[10] X. Liu, H. Guo, C. Ma, J. Power Sources 156 (2006) 267–280.
[11] H.P. Ma, H.M. Zhang, J. Hu, Y.H. Cai, B.L. Yi, J. Power Sources 162 (2006) 469–473.
[12] G. Li, P.G. Pickup, Electrochim. Acta 49 (2004) 4119–4126.
[13] M. Ciureanu, J. Appl. Electrochem. 34 (2004) 705–714.
[14] W.R. Mérida Donis. Diagnosis of PEMFC Stack Failures via Electrochemical Impedance Spectroscopy. PhD Dissertation. Department of Mechanical Engineering, University of Victoria, 2002.
[15] Y.-H. Chu, S.-W. Ahn, D.-Y. Kim, H.-J. Kim, Y.-G. Shul, H. Han, Catal. Today 111 (2006) 176–181.
[16] N. Wagner, E. Gulzow, J. Power Sources 127 (2004) 341–347.
[17] N. Wagner, M. Schulze, Electrochim. Acta 48 (2003) 3899–3907.
[18] I.M. Hsing, X. Wang, Y.-J. Leng, J. Electrochem. Soc. 149 (2002) A615–A621.
[19] F. Barbir, H. Gorgun, X. Wang, J. Power Sources 141 (2005) 96–101.
[20] W. He, G. Liu, T. Van Nguyen, AIChE J. 49 (2003) 3221–3228.
[21] X. Liu, H. Guo, F. Ye, C.F. Ma, Electrochim. Acta 52 (2007) 3607–3614.
[22] H. Yamada, T. Hatanaka, H. Murata, Y. Morimoto, J. Electrochem. Soc. 153 (2006) A1748–A1754.
[23] J. Stumper, M. Lohr, S. Hamada, J. Power Sources 143 (2005) 150–157.
[24] A.-M. Azad, Sens. Actuators B: Chem. 120 (2006) 25–34.
[25] A.-M. Azad, M. Hammoud, Sens. Actuators B: Chem. 119 (2006) 384–391.
[26] C.V. Gopal Reddy, P.K. Dutta, S.A. Akbar, Sens. Actuators B: Chem. 92 (2003) 351–355.
[27] S. Gottesfeld, J. Pafford, J. Electrochem. Soc. 135 (1988) 2651–2652.
[28] A. Hashimoto, T. Hibino, M. Sano, Electrochem. Solid-State Lett. 5 (2002) H1–H3.
[29] K.W. Kirby, A.C. Chu, K.C. Fuller, Sens. Actuators B: Chem. 95 (2003) 224–231.
[30] S. Kundu, M.W. Fowler, L.C. Simon, S. Grot, J. Power Sources 157 (2006) 650–656.
[31] R. Mukundan, E.L. Brosha, F.H. Garzon, Solid State Ionics 175 (2004) 497–501.
[32] D.P. Wilkinson, S.D. Knights, M.V. Lauritzen, Sensor Cell for an Eletrochemical Fuel Cell Stack. 2000, Ballard Power Systems Inc.: US 6,673,480. p. 59.

[33] D.P. Wilkinson, J. St-Pierre, J. Power Sources 113 (2003) 101–108.
[34] D.J.L. Brett, S. Atkins, N.P. Brandon, V. Vesovic, N. Vasileiadis, A. Kucernak, Electrochem. Solid-State Lett. 6 (2003) A63–A66.
[35] S.J.C. Cleghorn, C.R. Derouin, M.S. Wilson, S. Gottesfeld, J. Appl. Electrochem. 28 (1998) 663–672.
[36] M.M. Mench, C.Y. Wang, M. Ishikawa, J. Electrochem. Soc. 150 (2003) A1052–A1059.
[37] M. Noponen, T. Hottinen, T. Mennola, M. Mikkola, P. Lund, J. Appl. Electrochem. 32 (2002) 1081–1089.
[38] P.C. Rieke, N.E. Vanderborgh, J. Electrochem. Soc. 134 (1987) 1099–1104.
[39] I.A. Schneider, H. Kuhn, A. Wokaun, G.G. Scherer, J. Electrochem. Soc. 152 (2005) A2092–A2103.
[40] I.A. Schneider, H. Kuhn, A. Wokaun, G.G. Scherer, J. Electrochem. Soc. 152 (2005) A2383–A2389.
[41] J. Stumper, S.A. Campbell, D.P. Wilkinson, M.C. Johnson, M. Davis, Electrochim. Acta 43 (1998) 3773–3783.
[42] D.J. Ives, G.J. Janz, Reference Electrodes, in: Theory and Practice, N.Y.: Academic Press, 1961.